

Tridentate Pyrazole Ligands: Synthesis, Characterization and Corrosion Inhibition properties with Theoretical investigations

Y. Kaddouri^{1*}, A. Takfaoui¹, F. Abrigach¹, M. El Azzouzi², A. Zarrouk²,
F. El-Hajjaji³, R. Touzani^{1,4}, H. Sdassi⁵

¹ LCAE, COSTE, Faculty of sciences, University Mohammed 1st, BP. 717, 60 000 Oujda, Morocco

² LCA2ME, Faculty of sciences, University Mohammed 1st, BP. 717, 60 000 Oujda, Morocco

³ Laboratoire d'Ingénierie des Matériaux, de Modélisation et d'Environnement, LIMME, Faculté des Sciences DEM, Université Sidi Mohammed Ben Abdallah, USMBA, BP 1796, Atlas – Fès, Morocco.

⁴ Multidisciplinary Faculty, BP. 300, Selouane 62 702 Nador, Morocco

⁵ Laboratory of Bioorganic chemistry, Faculty of sciences, University Chouaib Doukkali, BP 20, 24 000 El Jadida

Received 11 Dec 2016,
Revised 30 Jan 2017,
Accepted 31 Jan 2017

Keywords

- ✓ Pyrazole
- ✓ Corrosion
- ✓ HCl
- ✓ Mild steel
- ✓ Weight loss
- ✓ Adsorption isotherm
- ✓ GAUSSIAN 09W
- ✓ EIS
- ✓ Tafel

Y. Kaddouri

Yassine.kaddouri92@gmail.com

Abstract

4-(bis((3,5-dimethyl-1H-pyrazol-1-yl) methyl) amino) benzonitrile (**L**₁) and 4-(bis((1H-pyrazol-1-yl) methyl) amino) benzonitrile (**L**₂) were prepared with good yields (up to 90 %), they were characterized using different physicochemical methods as FTIR, ¹H NMR, ¹³C NMR and MS. We have studied their inhibition efficiencies against corrosion of mild steel in molar hydrochloric acid solution by weight loss and electrochemical measurements. The inhibition efficiency using weight loss measurement reached 92.4 % for **L**₁ and 92.3 % for **L**₂ at the highest concentration 10⁻³. By studying the temperature effect, we conclude that the ligands were adsorbed according to Langmuir adsorption isotherm. And from polarization curves that all the ligands are mixed type inhibitors. The impedance diagrams in the Nyquist presentation shows that the corrosion is controlled by charge transfer process. We used GAUSSIAN 09W program to do theoretical investigations by considering the Density Functional Theory (DFT) method to calculate quantum parameters as E_{HOMO}, E_{LUMO}, ΔE_{HOMO}-E_{LUMO} and μ dipolar moment that allows us to confirm the experimental results.

1. Introduction

Steel is considered the most used as structural materials in the industries because of their good mechanical properties and low cost, but it's attacked by different aggressive environment as acidic, alkaline, salts ...etc. This attack named Corrosion, and it's an irreversible interfacial reaction between a material (metal for example) face to the environment [1]. The utility of inhibitors (organic or mineral) was considered the best option for the protection of metal face to the corrosion in a closed environment [2], that's why the searchers towards the synthesis of new chemical compounds. In this work, we are interested about tridentate pyrazolic ligands with N-C-N junction, which is one of the two types in common, several compounds have been already synthesized which are the same structure just they changed the substituents on the aromatic ring [3-7], the change of the substituents as on the pyrazoles or on the aromatic ring has effect on the inhibition efficiency, because there is a correlation between the molecular structure and the power on inhibition [8], the presence of donor substituents push the electronic density over the nitrogen atoms, these ligands have the ability to confer their anti-bonding electrons; of the nitrogen in the pyrazoles; with the protons to be adsorbed on the surface. The objective of this work is to study the relation between structure and inhibition efficiency by changing substituents which have different electronic effects causes an important change of electronic density that influence the inhibition efficiency.

2. Materials and methods

2.1. Synthesis of ligands

We have prepared four Ligand that are presented in the figure 1, then we have test them as corrosion inhibitors of mild steel in hydrochloric acid solution, they are synthesized according to the known experimental method [9-21] by condensation of one equivalent of substituted aniline with two equivalent of Hydroxy Methyl Pyrazole derivatives in acetonitrile as a polar solvent, the reactants are refluxed for four hours (Figure 1). The Ligand has been purified then characterized by FTIR, ^1H NMR, ^{13}C NMR spectroscopy and mass spectroscopy analysis.

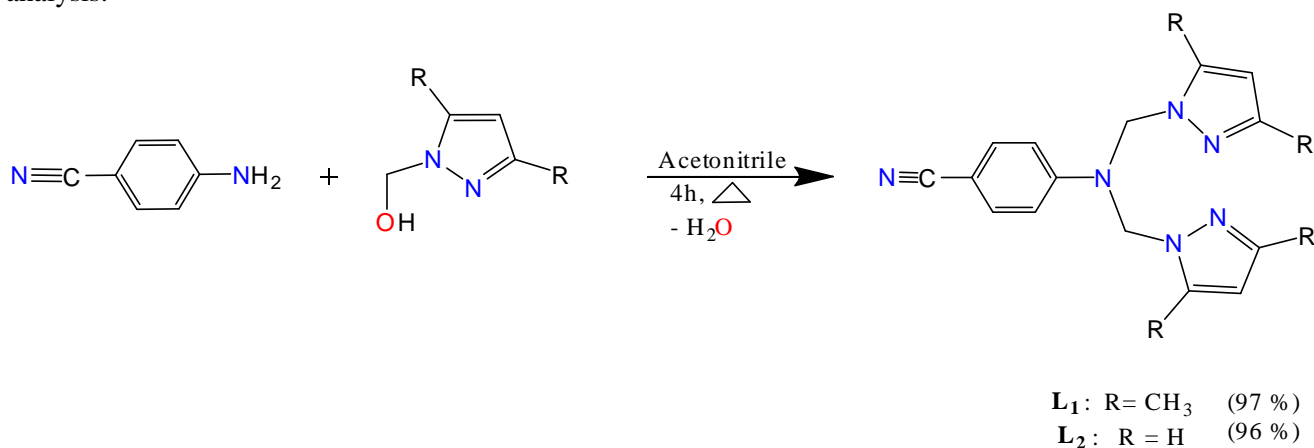


Figure 1. Synthesis of the ligands L_1 and L_2

2.2. Characterization of ligands

2.2.1. Chemical analysis

Nuclear magnetic resonance (NMR) spectroscopy, Fourier transforms infrared (FTIR) and Masse spectroscopy were used to verify the structure of the synthesized ligands. These compounds have spectral data according to the literature [3].

2.2.2. Materials and solutions

The steel that we used is mild steel with chemical composition (in wt%) of 99.21% Fe; 0.21% C; 0.38% Si; 0.09% P; 0.01% Al; 0.05% S and 0.05% Mn. We prepared rectangular simple of steel (length= 2 cm, width= 2 cm, thickness= 0.3 cm) as an electrode for weight loss measurements, they are grinding with emery paper SiC (60, 180, 240, 400, 600 and 1200), rinsed with double-distilled water and dried by hot air. The aggressive solution is prepared from 37% HCl analytical grade with double-distilled water.

2.2.3. Weight loss measurements

This is a simple and ancient experiment for corrosion study, just we need steel samples that we put indifferent concentrations of Ligand solution and the prepared aggressive solution as a blank, we put all the beakers containing the prepared solutions at 35 °C water bath for 6 hours, to get a good result we triplicate the experiment. After immersion of the steel specimens, they were rinsed with double-distilled water and then dried with hot air. The corrosion rate (v) is calculated using the following equation:

$$v = \frac{\Delta m}{S \times t} \quad (1)$$

where Δm is the average of weight loss of the three experiments, S the total area of the steel samples and t is the immersion time (6 hours). Then we are going to calculate from it the inhibition efficiency IE (%) as follows:

$$\text{IE} (\%) = \left(\frac{v_1 - v_2}{v_1} \right) \times 100 \quad (2)$$

Where v_1 and v_2 are respectively the values of corrosion rate in the absence and the presence of different concentration of the inhibitor.

2.2.4. Polarization measurements

All the measurements are controlled by computer using Voltmaster Program, using a double layer cell provided by three electrodes: Working electrode which is a circular steep sample ($S=1\text{cm}^2$), Auxiliary electrode of Platine and Reference electrode of saturated Calomel (ECS). The electrodes are associated to a potentiostat/galvanostat type PGZ 100, and a double frame thermostat (TACUSSEL standard CEC/TH) to make the temperature stable at $35\text{ }^\circ\text{C}$ by circulation of water to the cell.

2.2.4.1. Potentiodynamic polarization

Recording the potentiodynamic curves (anodic and cathodic) give us an overview of the mild steel electrochemical behavior. In the experiment, we put different concentration of the inhibitor present in the solution of HCl 1M, and before each experiment the working electrode which is a mild steel square sample was polished using emery paper (up to 1200). First of all, we start with the stabilization of the potential by immersing the working electrode which in the prepared concentration, to have a stable state open circuit potential in 30 min, then we record the Potentiodynamic curves by changing automatically the potential from -800 mV to -200 mV and a scan rate of 1 mV/s . The inhibition efficiency was calculated using the next equation: $IE(\%) =$

$$\frac{I_{\text{corr(Blank)}} - I_{\text{corr(inh)}}}{I_{\text{corr(Blank)}}} \times 100 \quad (3)$$

Or $I_{\text{corr(Blank)}}$ et $I_{\text{corr(inh)}}$ are the current density of corrosion for the mild steel without and with the addition of inhibitor which is one of the ligands L_1 and L_2 .

2.2.4.2. Electrochemical impedance spectroscopy (EIS)

The EIS diagrams in the Nyquist presentation was plotting after obtaining the corrosion potential by open circuit potential, by changing the frequencies from 100 to 10mV the computer draw 10 mV peak to peak. The inhibition efficiency was calculated using the next equation:

$$IE(\%) = \frac{R_{t(\text{inh})} - R_{t(\text{blank})}}{R_{t(\text{inh})}} \times 100 \quad (4)$$

$R_{t(\text{inh})}$ and $R_{t(\text{blank})}$ are the resistances of charge transfer of the solution with and without the presence of inhibitor in HCl 1M.

2.2.5. Theoretical studies

This method is widely used in quantum chemistry to confirm the experimental results, and have proven very powerful tools to study the corrosion inhibition mechanisms. [22,23] The measurement are performed using the GAUSSIAN 09W [24] suite by the DFT (density functional theory) method while adopting the functional hybrid B3LYP which use the three functional parameters of Becke (B3) and include the mixed exchanged terms of HF and DFT associated to the functional correlation gradient corrected of Lee, Yang and Parr (LYP), and the base is 6-31G (d,p). The geometry of the ligands is determined by optimization of all the geometric variables without any symmetry constraints. Then we are going to extract the quantum chemistry descriptors as E_{HOMO} , E_{LUMO} , the energy gap $\Delta E(\text{gap})$, dipole moment (μ), hardness (η), ionization energy (I), and the number of transferred charges ΔN .

3. Results and Discussion

Weight loss measurements

3.1.1. The concentration effect

It's clear from the Table 1 that the addition of the inhibitor molecules decreases the corrosion rate with the increase of their concentration. The data obtained show that the inhibition efficiency reaches the maximum at 10^{-3} M of both L_1 and L_2 . Examination of molecular structures reflects that L_1 and L_2 differ only by the substitution of hydrogen atom by methyl group. The quasi-similar inductive effect of H and CH_3 gave almost the same E% and consequently we can class them as: L_1 (% IE= 92.4%) \sim L_2 (% IE= 92.3%).

1.1.1. The temperature effect

It's essential to study the effect of temperature to know the steel behavior in the acidic environment (HCl 1M) and the metal/inhibitor interaction into the surface see Table 2.

Table 1. The corrosion rates and inhibitory efficiencies of the two ligands studied at different concentrations in 1M HCl

Inhibitors	Concentration	$V_{corr}(mg.cm^2.h^{-1})$	IE (%)
Blanc	1	0.940	
L_1	10^{-3}	0.0710	92.4
	5×10^{-4}	0.0891	90.5
	10^{-4}	0.1812	80.7
	5×10^{-5}	0.2216	76.4
	10^{-5}	0.2316	75.4
L_2	10^{-3}	0.0717	92.3
	5×10^{-4}	0.0843	91.1
	10^{-4}	0.0881	90.7
	5×10^{-5}	0.3113	66.9
	10^{-5}	0.5402	42.6

Table 2. The results of the corrosion rates and inhibitory efficiencies for the ligands L_1 and L_2

T(°C)	C(M)	L_1		L_2	
		$V_{corr}(mg.cm^2.h^{-1})$	IE (%)	$V_{corr}(mg.cm^2.h^{-1})$	IE (%)
40	Blanc	1.775			
	10^{-3}	0.4022	77.3	0.4702	79.1
50	Blanc	3.053			
	10^{-3}	0.7589	75.1	0.8054	73.6
60	Blanc	5.371			
	10^{-3}	1.9052	64.5	2.1529	64.8
70	Blanc	8.336			
	10^{-3}	4.4339	46.8	4.2155	49.4

Generally, the increase of temperature causes an acceleration of corrosion phenomena because it decreases the areas of stability of metals and accelerates the reaction and the transport kinetic[25]. We conclude from the table data that the increase of temperature break up the sensitive Van der Waals bonds that make physical interactions with the metal surface.

1.1.2. The activation thermodynamic parameters

This increase of temperature result desorption of inhibitors molecules, and the more important is for the inhibitors that contain fluorine as a substituent in ortho and para positions on the benzene. A lot of studies [26-28], show that the decrease of activation energy by the addition of inhibitor into the acidic solution is due to the growth of metal surface covered by the inhibitor molecules with the increase of temperature. We express the corrosion rate which depends on the temperature by the equation of Arrhenius: $V_{corr} = A \times e^{-\frac{E_a}{R.T}}$ (5)

$$\text{from where } \ln(V_{corr}) = \ln A - \frac{E_a}{R.T} \quad (6)$$

Or V_{corr} : the corrosion rate (mg/cm².h), E_a : the apparent activation energy (depends on the unit of the constant R), A: Arrhenius pre-exponential parameter, T: the absolute temperature (Kelvin), R: perfect gas constant and K a constant. We draw $\ln(V_{corr}) = f\left(\frac{1000}{T}\right)$ that give us a graphic straight with a slope: $-\frac{E_a}{R}$ which allows us to calculate E_a in absence of inhibitor ($E_a=46.49$ kJ/mol) that represent the energy barrier that should be crossed by the inhibitor to be adsorbed on the metal surface. To access the thermodynamic parameters of activation (the enthalpy of activation ΔH_a° and the entropy of activation ΔS_a°), we use the Arrhenius equation of transition [29]:

$$V_{corr} = \frac{RT}{N_A h} \times \exp\left(\frac{\Delta S_a^\circ}{R}\right) \times \exp\left(-\frac{\Delta H_a^\circ}{RT}\right) \quad (7)$$

Or h : Plank constant, N_A : Avogadro number, ΔH_a° : the enthalpy of activation and ΔS_a° : the entropy of activation (Table 3).

Table 3. The thermodynamic parameter values of activation for mild steel in 1 M HCl in the absence and presence of ligands L_1 and L_2

	C (M)	E_a (kJ/mol)	ΔH_a° (kJ/mol)	ΔS_a° (kJ/mol.K)	$E_a - \Delta H_a^\circ$ (kJ/mol)
	Blanc	46.49	43.77	-100.60	2.72
L_1	10^{-3}	79.59	76.87	-9.56	2.72
L_2	10^{-3}	72.63	69.91	-30.42	2.72

By the ranking of Radovici [29], the results of the activation energy collected in the table are upper with the inhibitor than without them. That could be attributed to the adsorption of inhibitor molecules on the surface of the metal, which decrease the interactions between the corrosive environment and the surface of the metal. About the ΔH_a° values which are positive reflect the endothermic nature of the mild steel dissolution process, also blocked because their values are bigger with the inhibitor than without. The activation energy values are bigger than ΔH_a° which indicate that the corrosion process involve a gas phase, it's the formation of H_2 .

1.1.3. The adsorption isotherm

The adsorption characteristics study is very important to know the electrochemical process on the surface of the metal; this study will give us an idea about the aptitude of the molecule to fix on the steel surface [30]. To get a view of the adsorption process we go to use several adsorption isotherms as Langmuir [31], Freundlich [32], Temkin [33], Florry-Huggins [34], Frumkin [35], Adejo-Ekwenchi [36] and El-Awady [37]. These isotherms link the surface coverage (θ)(8) with the inhibitor concentration C_{inh} .

$$\theta = \frac{V_{corr} - V_{corr(inh)}}{V_{corr}} \quad (8)$$

To find the corresponding isotherm for each inhibitor, we compare the correlation coefficients (R^2) that are assembling in the Table 5:

Table 5. The correlation coefficient R^2 values obtained for each isotherm and each ligand studied inhibitor

	Adsorption isotherms						
	Langmuir	Freundlich	Temkin	Florry-Huggins	Frumkin	Adejo-Ekwenchi	El-Awady
L_1	0.9998	0.9198	0.915	0.8775	0.8031	0.8868	0.8933
L_2	0.9765	0.7908	0.81	0.5478	0.1862	0.8274	0.8308

By the table data, we conclude that the inhibitors L_1 and L_2 with the correlation coefficients values 0.9998 and 0.9765 obey the Langmuir isotherm in the molar Hydrochloric acid (HCl 1M) (Figure 2).

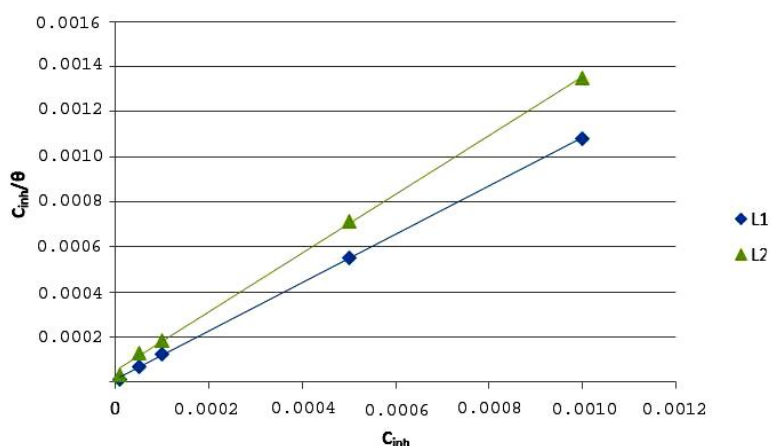


Figure 2. Trace of adsorption isotherm curves for the ligands L_1 and L_2

After obtaining these results we go to reveal the thermodynamic parameters of our inhibitors using the Langmuir adsorption isotherm. We will calculate the standard adsorption free energy by the next equation:

$$\Delta G^{\circ}_{ads} = -RT \ln(55.5 K_{ads}) \quad (9)$$

And ΔG°_{ads} : the standard adsorption free energy, R: constant of the perfect gas, T: The absolute temperature in Celsius ($^{\circ}C$), 55.5 the concentration of water in solution in mol/dm^3 , K_{ads} : Equilibrium constant for adsorption process. The results are assembling in the Table 6:

Table 6. The thermodynamic parameters obtained for the inhibitor molecules L_1 and L_2

	Adsorption isotherm	K_{ads}	ΔG°_{ads} (kJ/mol)
L_1	Langmuir	92336.10	-39.56
L_2		4182.70	-31.64

The K_{ads} values are positives and big, so it gives us the information about the strong interactions between the inhibitor molecules and the metal surface. The ΔG°_{ads} values are between -20 kJ/mol and -40 kJ/mol so all the inhibitors are physisorbed and chemisorbed. They are negatives, so it shows us that reaction is spontaneous and that our inhibitors L_1 and L_2 form a monolayer on the metal surface.

1.2. Polarization measurements

1.2.1. Potentiodynamic polarization

From the Table 7 and Figure 3, we conclude that the corrosion current density I_{corr} values for the steel in acidic environment with the presence of the inhibitor are lower than those without (blank). We note that the addition of the inhibitor the hydrochloric environment causes the decrease of the corrosion current density and also of Tafel slopes β_c and β_a . In our case, the cathodic curves present a linear part indicates that reaction of the reduction of H_2 on the metal surface is made according to pure activation mechanism. The anodic curves show that the inhibition mode depends on the electrode potential. In fact, for an overvoltage superior than -300mV/ECS, the presence of the inhibitors in the solution don't affect the anodic I-E curves that appear overlapped with that of the blank, suggesting the inhibitor desorption and therefore the dissolution dominates the anodic reaction. The marked decrease of the cathodic current density and in more negative potentials than -300mV/ECS, in the

anodic range, plus the slight shift of the free potential towards the lower nobles values, shows that studied inhibitors are mixed type with a predominance cathodic. The inhibitory efficacy of the tested compounds increases the following order: L_1 (% IE = 97.57%) ~ L_2 (%IE = 94.69 %).

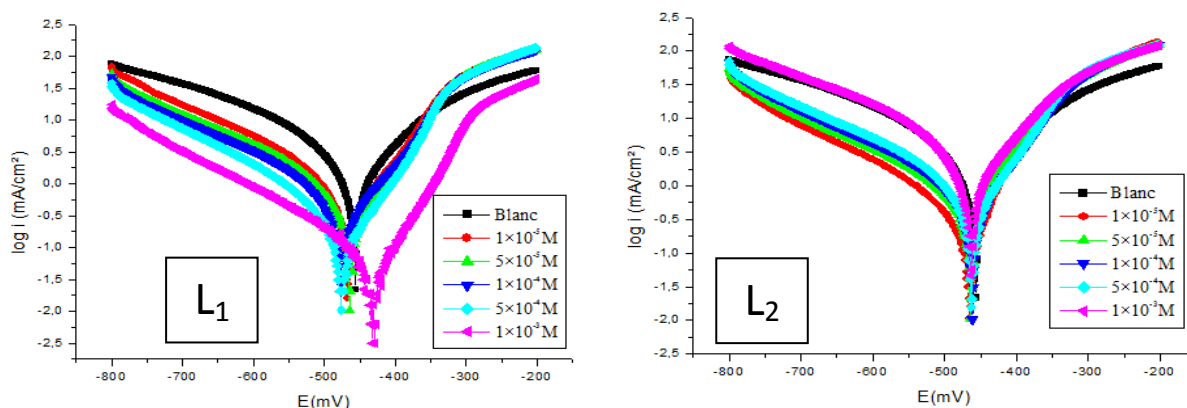


Figure 3. The polarization curves of mild steel in HCl without and with addition of different concentrations of L_1 and L_2

Table 7. The electrochemical parameters and inhibition efficiency of the corrosion of mild steel in 1M HCl for different concentrations L_1 and L_2 .

Inhibitor	C(M)	E_{corr} (mV/SCE)	β_c (mV/dec)	β_a (mV/dec)	I_{corr} (μ A/cm ²)	IE (%)
Blanc	1	-457.3	-218	172.5	3280.8	
L_1	1×10^{-3}	-431.9	-161.4	62.6	79.7	97.57
	5×10^{-4}	-476.6	-181.4	84.3	429.9	86.9
	1×10^{-4}	-464.1	-203	91.7	860	73.88
	5×10^{-5}	-476	-214.6	100.7	868	73.54
	1×10^{-5}	-467	-206.9	102.8	1286.1	60.8
L_2	1×10^{-3}	-447.3	-96.7	63.1	174.3	94.69
	5×10^{-4}	-459.6	-86.5	73	250.9	92.35
	1×10^{-4}	-461.5	-90.2	73.9	467	85.76
	5×10^{-5}	-459	-178.1	111.3	706.2	78.47
	1×10^{-5}	-463.5	-87.4	79.8	786.8	76.01

1.2.2. Electrochemical impedance spectroscopy (EIS)

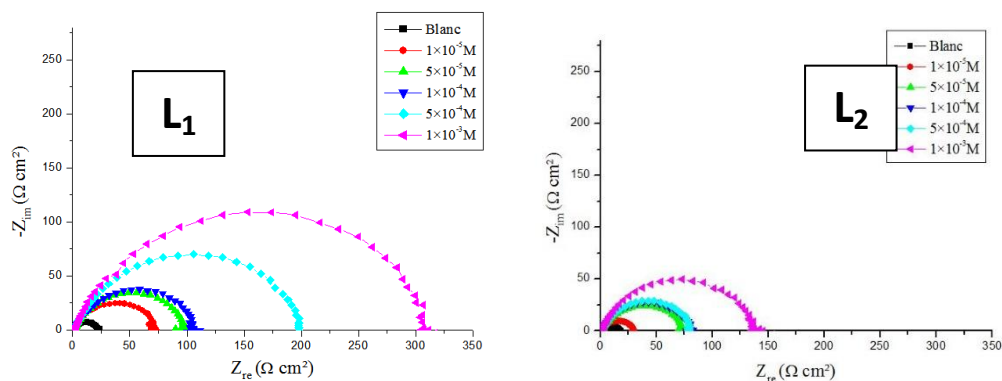


Figure 4. The impedance diagrams for the inhibitors L_1 and L_2

We see in Figure 4 that all the EIS curves are constituted of one half loop, so generally the corrosion reaction is controlled by a charge transfer process on a solid electrode that have a heterogeneous and irregular surface see Table 8.

Table 8. The electrochemical parameters of mild steel impedance diagram in 1M HCl in the presence of ligands at various concentrations obtained E_{corr} (T = 35 °C)

Inhibitor	C(M)	R_{Ω} ($\Omega \cdot \text{cm}^2$)	R_t ($\Omega \cdot \text{cm}^2$)	F_{\max} (Hz)	C_{dl} ($\mu\text{F}/\text{cm}^2$)	IE (%)
Blanc	1	1.996	14.994	63.29	167.79	
L_1	1×10^{-3}	1.921	332.6	7.93	62.61	95.32
	5×10^{-4}	1.436	204	10	78.61	92.6
	1×10^{-4}	1.779	108.12	15.82	93.09	86.13
	5×10^{-5}	1.655	98.44	15.82	102.24	84.77
	1×10^{-5}	1.456	45.46	25	140.11	79.66
L_2	1×10^{-3}	1.564	138.74	15.82	72.55	89.19
	5×10^{-4}	1.631	81.85	25	77.82	81.68
	1×10^{-4}	1.46	79.73	20	99.86	81.19
	5×10^{-5}	1.438	75.95	20	104.82	80.26
	1×10^{-5}	1.536	28.90	50	110.18	48.12

The R_t values and the inhibition efficiency IE (%) become more important with the increase of the inhibitor concentration the aggressive solution. The double layer capacity (C_{dl}) values decrease with the increase of the inhibitor concentration; this is due to the inhibitor molecules adsorption on the metal surface, causing the decrease of their active surface. Therefore, more the inhibitor is adsorbed more the thickness of the organic deposit is bigger and also the double layer capacity decrease according to the expression of C_{dl} presented in Helmotz model: $C_{dl} = \frac{\epsilon_0 \epsilon}{e} S$ (10) Or e is the thickness of the deposit, S is the electrode surface, ϵ_0 is the permittivity of the medium and ϵ is the dielectric constant. This change in R_t and C_{dl} is probably due to the displacement of water molecules by the Cl^- ions of the acid and the adsorption of organic molecules onto the metal surface, decreasing the metal dissolution reaction rate and reduction H^+ protons.

1.2.3. Equivalent electric circuit (EEC)

In the immediate vicinity of the interface, the high electric field brings up a space charge (double layer) and leads to the parallel of a capacitor C , with the Faraday impedance. The equivalent electrical circuit (EEC) representative in the case of adsorption of inhibitors ligands is shown in Figure 5. This circuit consists of a constant phase element (CPE), used instead of a capacitor to account for heterogeneities of a surface of the electrode resulting from the surface roughness, impurities, dislocations grain boundaries, adsorption inhibitors, and the formation of porous layers [38] of the electrolyte resistance (R_{Ω}) and the charge transfer resistance (R_t).

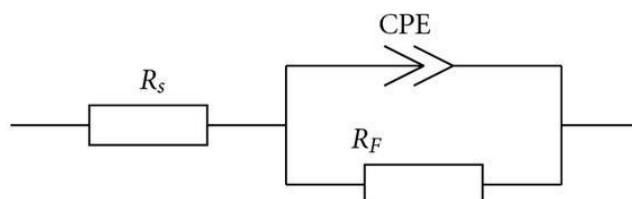


Figure 5. Electrical equivalent circuit of steel interface / ligand / HCl

The choice of 10^{-3} M concentration is justified by the fact that at this concentration, the value of inhibition efficiency is the maximum. An excellent parametric adjustment of experimental loops impedances whole series of ligands (L_1 and L_2) was obtained using the new model. Experimental and stimulated diagrams are well correlated. The values of different parameters from the parametric adjustment using the EC-Lab ® software program (Version 11.01) are listed in the Table 9.

Table 9. The values of different parameters from the parametric adjustment by EC-Lab ® software

Inhibiteur	R_1 (Ohm)	R_2 (Ohm)	C (μ F)
Blanc	0.9876	7.529	286
L_1	1.102	152.5	128.1
L_2	0.7837	67.28	128.2

Taking into account heterogeneities of our working electrode resulting from the roughness of its surface, dislocations, along grains, adsorption inhibitors, and the formation of porous layers [39], the double layer capacitance is affected, it is for this effect is simulated a constant phase element (CPE) [40]. This element is assigned to give a precise adjustment [41], which is the case we obtained that digraphs adjusted correlate perfectly with those experimental.

1.3. Theoretical studies

1.3.1. DFT method

1.3.1.1. Structure optimization

Using the density functional theory (DFT) by GAUSSIAN 09W, considering the inhibitors in their isolate state in the B3LYP/6-31 G (d, p). The optimized structures for the synthesized inhibitors are represented in the Figure 6.

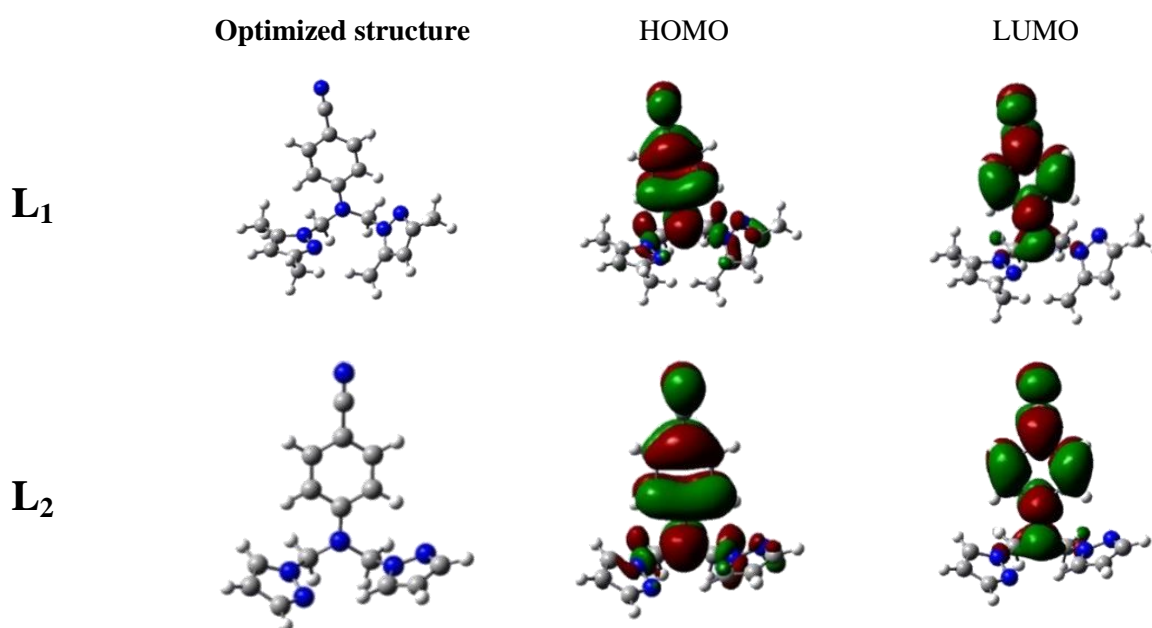


Figure 6. The optimized structures and their HOMO, LUMO representation of L_1 and L_2 .

1.3.1.2. Quantum parameters

We experimentally class the inhibition efficiency of our synthesized ligands and we have this order: $L_1 > L_2$. To verify these results and compare it with those obtained experimentally, we are going to do theoretical investigation, using the DFT method we will calculate different quantum parameters that will give us a theoretical order of the four inhibitors L_1 and L_2 . We define the calculated parameters by these equations:

$$\Delta E(\text{gap}) = E_{\text{HOMO}} - E_{\text{LUMO}} \quad (11)$$

By the Koopmans theory [41] we have: $I = -E_{\text{HOMO}}$ (12) and $A = -E_{\text{LUMO}}$ (13) and $\eta = \frac{I-A}{2}$ (14)

By the Pearson scale of electronegativity [42] we calculate the number of electron transferred as:

$$\Delta N = \frac{\chi_{\text{Fe}} - \chi_{\text{inh}}}{2(\eta_{\text{Fe}} - \eta_{\text{inh}})} \quad (12)$$

Table 10. The values of the descriptors of quantum chemistry found after geometrical optimization GAUSSIAN 09W and those calculated

Quantum parameters	E_{HOMO}	E_{LUMO}	$\Delta E_{(\text{gap})}$	μ	I	η	ΔN
L_1	-0.21696	-0.02925	0.18771	8.4609	0.21696	0.093855	-0.32271549
L_2	-0.22624	-0.03715	0.18909	7.0132	0.22624	0.094545	-0.32468195

1.3.1.3. E_{HOMO} and E_{LUMO}

The molecular orbital HOMO, is the highest occupied orbital (in energy), so it's energetically the easiest to give electron. The molecular orbital LUMO, is the lowest unoccupied orbital (in energy), so it's energetically the easiest to accept electron on it's orbital. The molecular orbitals HOMO and LUMO could be used to predict the centers of adsorption in the inhibitor molecules [43-46]. Examining these two parameters, we note that L_1 is more donor than L_2 because of the presence of four substituents (methyl) on the two pyrazoles in its molecular structure.

1.3.1.4. Energy gap

The gap between the energetic levels HOMO and LUMO of our ligands, $\Delta E_{(\text{gap})} = E_{\text{HOMO}} - E_{\text{LUMO}}$, is another important quantum parameter which should be considered in the quantum chemistry [47]. The energy gap describes the necessary energy to do the first excitation, thus the inhibition efficiency of the corrosion is inversely proportional with the energy gap value. We conclude from the energy gap values of the four ligands that L_1 is the easiest molecule that could be excited.

1.3.1.5. Ionization energy

The ionization energy (I) is a fundamental descriptor for chemical reactivity of atoms and molecules. The biggest ionization energy value indicates the stability and the chemical inertness, and the lowest value indicates the highest reactivity of atoms and molecules [48]. The lowest value of ionization energy for L_1 indicates the highest reactivity.

1.3.1.6. Hardness

The absolute hardness reflects the resistance of a system faces to the change of their electrons number. The lowest value of hardness means that is easy for the molecule to assign or capture electrons, and this is the case of L_1 .

1.3.1.7. Number of electron transferred

More the number of electrons transferred are bigger plus the adsorption on the metal surface is promoted, and this case of L_1 . These results can lead to increase adsorption on the metal surface and increase consequently the inhibition efficiencies. Related with the experimental inhibition efficiency, all the descriptors are well correlated with the inhibition efficiencies. By previous results, the best inhibitor is L_1 because of the four substituents (methyl) attached with the two pyrazoles in the structure, they are electro donors so they give electrons to the centers of adsorption on the inhibitor molecules (in this case is the nitrogen atom).

Conclusion

We conclude that L_1 is the best inhibitor due to the presence of methyl substituents on the pyrazole that increase the electronic density on the nitrogen atom, which is protonated by the acidic medium to facilitate the formation of bonding with the metal, so the adsorption of the molecules on the surface of the metal, which is physisorbed and chemisorbed. By changing temperature, we prove that L_1 obeys the Langmuir isotherm adsorption. Then by electrochemical methods, we see that from the polarization curves that L_1 and L_2 are mixed inhibitors. They reduce the speed of the two partial reactions but change little corrosion potential. The measured electrochemical impedances show that the Nyquist diagrams obtained show a single capacitive loop whose size increases in proportionate with the concentration of the inhibitor, indicating that corrosion of steel in acidic solution HCl 1M is essentially controlled by a process of charge transfer. Theoretical calculations show that the molecules having a high dipole moment exhibit good inhibitory efficacy.

References

1. Adejo S. O., Yiase S. G., Ahile U. J., Tyohemba T. G. and Gbertyo J. A., *Appl. Sci. Res.*, 5 (2013) 25-32.
2. Southon I. W., Buckingham J. (Eds.), « *Dictionary of Alkaloids* » Chapman & Hall, New York (1989).
3. Touzani R., Ramdani A., Ben-Hadda T., El Kadiri S., Maury O., Le Bozec H., Diwneuf P.H., *synth. Commun.*, 31 (9) (2001) 1315-1321.
4. Tebbji K., Oudda H., Hammouti B., Benkaddour M., El kodadi M., Malek F., Ramdani A., *App. Surf. Sci.* 241 (2005) 326–334.
5. Elayyachy M., Elkodadi M., Aouniti A., Ramdani A., Hammouti B., Malek F., Elidrissi A., *Mater. Chem. & Phy.* 93 (2005) 281–285.
6. Tebbji K., Aouniti A., Benkaddour M., Oudda H., Bouabdallah I., Hammouti B., Ramdani A., *Progr. in Org. Coat.* 54 (2005) 170–174.
7. Tebbji K., Bouabdallah I., Aouniti A., Hammouti B., Oudda H., Benkaddour M., Ramdani A., *Mater. Lett.* 61 (2007) 799–804.
8. Dafali A., Hammouti B., Mokhlisse R., Kertit S., Elkacemi K., *Corros. Sci.* 45 (2003) 1619–1630.
9. Abrigach, F., Bouchal, B., Riant, O., Mace, Y., Takfaoui, A., Radi, S., Oussaid, A., Bellaoui, M., Touzani, R., *Med. Chem.*, 12 (2016) 83-89.
10. El Ouafi A., Hammouti B., Oudda H., Kertit S., Touzani R., Ramdani A., *Anti-Corros.Meth.Mater.* 49 (2002) 199-204.
11. Dafali A., Hammouti B., Touzani R., Kertit S., Ramdani A., El Kacemi K., *AntiCorros.Meth.Mater.* 49 (2002) 96-104.
12. Touzani R., Garbacia S., Lavastre O., Yadav V.K., Carboni B., *J. Comb. Chem.* 5 (2003) 375-378.
13. Garbacia S., Hillairet C., Touzani R., Lavastre O., *Collec. Czech. Chem. Commun.* 70 (2005) 34-40.
14. Bouabdallah I., Zidane I., Hacht B., Touzani R., Ramdani A., *Arkivoc* 11 (2006) 1-7.
15. Bouabdallah I., Touzani R., Zidane I., Ramdani A., *Catal. Commun.* 8 (2007) 707-712.
16. Bouabdallah I., Touzani R., Zidane I., Ramdani A., *J. Iran. Chem. Soc.* 3 (2007) 299-303.
17. El Kodadi M., Malek F., Touzani R., Ramdani A., *Catal. Commun.* 9 (2008) 966-969.
18. Boussalah N., Touzani R., Bouabdallah I., El Kadiri S., Ghalem S., *J. Mol. Catal. A Chem.* 306 (2009) 113-117.
19. Touzani R., Ramdani A., El Kadiri S., *Inter. J. Phys. Sci.* 4 (2009) 906-907.
20. Zerrouki A., Touzani R., El Kadiri S., *Arab. J. Chem.* 4 (2011) 459-464.
21. Toubi Y., Touzani R., Radi S., El Kadiri S., *J. Environ. Mater. Sci.* 3 (2012) 328-341.
22. Ben Hmamou D., Aouad M. R., Salghi R., Zarrouk A., Assouag M., Benali O., Messali M., Zarrok H., Hammouti B., *J. Chem. Pharm. Res.* 4 (2012) 3489.
23. Zarrok H., Oudda H., El Midaoui A., Zarrouk A., Hammouti B., EbnTouhami M., Attayibat A., Radi S., Touzani R., *Res. Chem. Inter.*, 38 (2012) 2051-2063.

24. Gaussian 09, Revision A.02, Frisch M. J., Trucks G. W., Schlegel H. B., Scuseria G. E., Robb M. A., Cheeseman J. R., Scalmani G., Barone V., Mennucci B., Petersson G. A., Nakatsuji H., Caricato M., Li X., Hratchian H. P., Izmaylov A. F., Bloino J., Zheng G., Sonnenberg J. L., Hada M., Ehara M., Toyota K., Fukuda R., Hasegawa J., Ishida M., Nakajima T., Honda Y., Kitao O., Nakai H., Vreven T., Montgomery J. A., Jr., Peralta J. E., Ogliaro F., Bearpark M., Heyd J. J., Brothers E., Kudin K. N., Staroverov V. N., Kobayashi R., Normand J., Raghavachari K., Rendell A., Burant J. C., Iyengar S. S., Tomasi J., Cossi M., Rega N., Millam J. M., Klene M., Knox J. E., Cross J. B., Bakken V., Adamo C., Jaramillo J., Gomperts R., Stratmann R. E., Yazyev O., Austin A. J., Cammi R., Pomelli C., Ochterski J. W., Martin R. L., Morokuma K., Zakrzewski V. G., Voth G. A., Salvador P., Dannenberg J. J., Dapprich S., Daniels A. D., Farkas O., Foresman J. B., Ortiz J. V., Cioslowski J., and Fox D. J., *Gaussian, Inc., Wallingford CT* (2009).
25. Ammar I.A., El Khorafi F.M., *Werkst. und Korros.* 24 (1973) 702.
26. Benali O., Larabi L., Tabti B., Harek Y., *Anti-Corros Met Mat.*, 52 (2005) 280-285.
27. Benali O., Mokhtar O., *Arab. J. Chem.*, 4 (2011) 443-448.
28. Eddy N.O., Ebenso E.E., *Afri J of Pure & Appl Chem* 2 (2008) 1.
29. Radovici O., Proc. 7 th *Europ. Symp. on Corros. Inhib.*, Ann. Univ. Ferrara, Italy, (1990) 330.
30. Vermeulan T.H., Vermeulan K.R. and Hall.L.C. « *Fundamental* » *Ind. Eng. Chem.* 5 (1966) 212-223
31. Oguzie E.E., Njoku V.O., Enenebeaku C.K., Akalezi C.O., Obi C., *Corros. Sci.* 50 (2008) 3480-3486.
32. Freundlich H. M. F., Over the adsorption in solution, *J. Phys. Chem.* 57 (1906) 385-471.
33. Landolt D., *Corrosion et Chimie de Surface des Métaux, 1st Ed, Alden Press, Oxford* (1993) 495.
34. Frumkin A. N., *Progress in Surface Science*, 8 (1977) 1-2.
35. Adejo S. O., Ekwenchi M. M., *IOSR J. of Appli. Chem* (2014) 66-71.
36. Obot I.B., Obi-Egbedi N.O. and Umoren S.A., *Inter. J. of Electrochem. Sci.*, 4 (2009) 863-877.
37. Mc cafferty E., *Corrosion Control by coating, Science Press, Princeton* (1979).
38. Popova A., Sokolova E., Raicheva S., Christov M., *Corros. Sci.*, 45 (2003) 33.
39. Bommersbach P., Alemany-Dumont C., Millet J.P. et col; *Electrochim. Acta.*, 51 (2006) 4011
40. Macdonald J.R., Johanson W.B., in: J.R. Macdonald (Ed.); *Theory in impedance spectroscopy, John Wiley & Sons, New York.*, (1987)
41. Sastri V.S., Perumareddi J.R., *Corrosion*, 53 (1997) 617.
42. Fukui K., Yonezawa T., Shingu H., *J. Chem. Phys.*, 20 (1952) 722.
43. Guan N. M., Xueming L., Fei L.; *Mater. Chem. Phys.*, 86 (2004) 59.
44. Langmuir I.; *J. Am. Chem. Soc.*, 39 (1917) 1848.
45. Khamis K., *Corrosion Science*, 46 (1990) 476.
46. Umoren, S.A; *Arabic. Cellulose.*, 15 (2008) 751.
47. Senhaji O., Taouil R., Skalli MK. et al., *Int. J. Electrochem. Sci.*, 6 (2011) 6290.
48. Sandip K.R., Nazmul I., Dulal C.G., *J. Quant. Infor. Sci.* 1 (2011) 87-95.

(2017) ; <http://www.jmaterenvirosci.com/>